Bridging Simulation and Competition: A Systematic CFD Analysis of Aerodynamic Performance in CO_2-Powered Dragsters

Parjanya Vedula

Abstract

This study presents a comprehensive aerodynamic analysis of a CO_2-powered dragster using high-fidelity computational fluid dynamics (CFD). The research focuses on establishing a robust and accurate simulation methodology to guide design optimization for competitive racing. Key parameters including computational domain sizing, mesh refinement strategy, and the implementation of realistic boundary conditions such as wheel rotation and a moving ground plane are systematically investigated. The analysis identifies and examines critical aerodynamic phenomena, including the formation of dominant twin vortex structures in the vehicle's wake, extensive wake turbulence, and the pressure distributions driving drag.

A baseline simulation using coarse settings and non-rotating wheels yielded a total drag of -0.085 N, highlighting a significant underprediction of aerodynamic load. By systematically refining the methodology—implementing a finer mesh (Level 5), rotating wheels, and optimizing the computational floor length—the simulation's predictive accuracy was vastly improved. The final optimized design configuration achieved a total drag force of -0.132 N at a peak velocity of 28 m/s. While this represents a 22% aerodynamic improvement over initial refined concepts (-0.169 N), it remains higher than the 0.06–0.08 N drag forces reported for national championship-winning designs, indicating specific areas for further optimization. The paper concludes by providing a component-level drag breakdown and offering a framework for future design enhancements and advanced simulation work.

Nomenclature

Symbol	Description	Unit
D	Total Aerodynamic Drag Force	N
C_d	Coefficient of Drag	Dimensionless
ρ	Density of Air	kg/m³
v or U	Vehicle Velocity	m/s
A	Frontal Cross-Sectional Area	m²
R_e	Reynolds Number	Dimensionless
L	Characteristic Length	m
μ	Dynamic Viscosity of Air	Pa·s
ω	Angular Velocity of Wheel	rad/s
r	Wheel Radius	m
CFD	Computational Fluid Dynamics	-
RANS	Reynolds-Averaged Navier-Stokes	-
SST	Shear Stress Transport (Turbulence Model)	-

1. Introduction

1.1. Competition Context and Motivation

Student engineering competitions such as F1 in Schools and the Technology Student Association (TSA) Dragster Design challenge have become premier platforms for promoting STEM education. These competitions require teams to design, analyze, manufacture, and race miniature vehicles. The CO_2 dragster, a small-scale vehicle powered by the thrust from a standardized 8-gram CO_2 cartridge, is a cornerstone of these events. Races are conducted on a 20-meter tethered track, where victory is often decided by milliseconds. Winning times at the national level frequently fall within the 0.9–1.0 second range, a testament to the extreme level of optimization required.

1.2. The Primacy of Aerodynamics

While vehicle performance is a multifactorial problem dependent on mass, rolling resistance, launch mechanics, and alignment, aerodynamic drag emerges as the dominant resistive force at the high velocities achieved. As the vehicle accelerates, the drag force increases with the square of its velocity. At a typical peak velocity of 28 m/s (approximately 100 km/h or 63 mph), minimizing aerodynamic resistance is paramount to achieving a winning time. The most competitive designs exhibit total drag forces in the range of 0.06–0.08 N, whereas novice designs can easily exceed 0.2 N. This threefold difference underscores the profound impact of sophisticated aerodynamic design.

1.3. Research Objectives and Paper Structure

The primary objective of this research is to develop and validate a high-fidelity Computational Fluid Dynamics (CFD) methodology for accurately predicting the aerodynamic performance of a CO_2 dragster. Many student teams rely on CFD, but often without a systematic understanding of the simulation parameters required for results to correlate with reality. Inaccurate simulations can lead to misguided design decisions and poor on-track performance.

This paper seeks to address this gap by:

1. **Establishing** the governing physical principles relevant to dragster aerodynamics.
2. **Detailing** a systematic CFD methodology, with a focus on the impact of domain size, mesh refinement, and the modeling of wheel rotation.
3. **Analyzing** the results of a parametric study to quantify the sensitivity of drag prediction to these methodological choices.
4. **Investigating** the complex flow structures, such as wake vortices and pressure zones, that contribute to drag.
5. **Connecting** simulation insights to practical hardware choices and

benchmarking the design against elite performance standards.

The paper is structured as follows: Section 2 outlines the theoretical framework. Section 3 describes the computational methodology. Section 4 presents and discusses the results. Section 5 bridges the simulation work with real-world considerations. Finally, Section 6 provides conclusions and directions for future work.

---

2. Theoretical Framework and Governing Principles

2.1. The Physics of Aerodynamic Drag

Aerodynamic drag (D) is the force that resists an object's motion through a fluid. It is generated by the interaction between the object's surface and the fluid. The total drag force is calculated using the standard drag equation:

$$D = ½ \rho v^2 C_d \text{ A}$$

Where:

- ρ is the density of the fluid (air, ~1.225 kg/m³ at sea level).
- v is the velocity of the object relative to the fluid.
- C_d is the coefficient of drag, a dimensionless number that depends on the object's shape and surface roughness.
- A is the frontal cross-sectional area of the object.

For a CO_2 dragster, total drag is primarily composed of two components:

- **Pressure Drag (or Form Drag):** This is caused by a pressure differential between the front and rear of the vehicle. High pressure builds at the stagnation point on the nose, while a region of low-pressure, turbulent wake forms at the rear due to flow separation. This pressure difference creates a net force opposing motion. For bluff bodies and imperfectly streamlined shapes like a dragster, pressure drag is the dominant contributor.
- **Skin Friction Drag:** This arises from the shear stress of the fluid moving across the vehicle's "skin" or surface. It is a function of the wetted area (total surface area in contact with the flow) and the state of the boundary layer (laminar or turbulent).

2.2. Reynolds Number and Flow Regime Analysis

The Reynolds number (R_e) is a critical dimensionless quantity in fluid dynamics that describes the ratio of inertial forces to viscous forces. It helps predict the flow pattern and determine whether the flow will be laminar (smooth, layered) or turbulent (chaotic, vortical). It is calculated as:

$$R_e = \rho v L \mu$$

Where L is a characteristic length of the object and mu is the dynamic viscosity of the fluid (~1.81times10−5 Pa·s for air).

For the dragster, with a body length $L \approx 17$ m and peak velocity $v = 28$ m/s, the overall Reynolds number is:

R_e body $\approx 1.81 \times 10^{-5} \times 1.225 \times 28 \times 0.17 \approx 323{,}000$

This value indicates that the flow over the majority of the vehicle body is fully turbulent. However, different components operate under different local Reynolds numbers, affecting their individual flow regimes:

Table of Reynolds Number Scaling by Component

Component	Characteristic Length (m)	Reynolds Number (R_e)	Predicted Flow Regime
Nose Cone Tip	0.05	~95,000	Transitional / Turbulent Onset
Vehicle Body	0.17	~323,000	Fully Turbulent
Wheel Diameter	0.035	~66,000	Transitional (rotation critical)
Exposed Axle	0.012	~18,900	Laminar-to-Turbulent Transition

This analysis implies that the nose and wheels are particularly sensitive to geometry and surface finish, as their flow is in a transitional state where small changes can trigger or delay the shift to turbulence, significantly affecting drag.

2.3. Key Aerodynamic Phenomena

CFD analysis reveals several complex flow phenomena critical to dragster performance:

- **Wake Turbulence:** The region of recirculating, low-pressure flow behind the vehicle is known as the wake. A large, energetic wake signifies a large pressure difference between the vehicle's front and rear, resulting in high pressure drag. The goal of rear-body design (e.g., using a diffuser) is to manage flow separation and promote pressure recovery, thereby shrinking and weakening the wake.

- **Twin Vortex Drag Zones:** A common feature observed in ground vehicles is the formation of two large, counter-rotating vortices that originate from the sharp edges of the rear body or wheels. These structures entrain energy and sustain the low-pressure region, acting as major contributors to drag. Their strength and stability are highly dependent on the vehicle's rear-end geometry.
- **Unsteady Turbulence:** Flow over the dragster is not perfectly steady. Vortices can be shed periodically from sharp edges, a phenomenon known as vortex shedding. This creates oscillating forces on the body and can lead to an increase in the time-averaged drag compared to a hypothetical steady flow.

2.4. The Critical Role of Wheel Dynamics

The wheels of a CO_2 dragster rotate at extremely high speeds. The angular velocity (ω) is given by ω = vr. At a peak velocity of 28 m/s:

- **Front Wheels** (r ≈ 0.015 m): $\omega \approx$ 1866 rad/s, or ~17,800 RPM.
- **Rear Wheels** ($r \approx 0.0175$ m): $\omega \approx$ 1600 rad/s, or ~15,300 RPM.

This rotation fundamentally alters the aerodynamics:

- The top surface of the wheel moves at twice the vehicle's speed relative to the surrounding air ($v + \omega r = 2v$).
- The bottom surface is momentarily stationary relative to the ground.
- This asymmetry creates a "jetting" effect on the sides and throws air into the wheel wells and wake, generating significant turbulence. Simulating wheels as static (non-rotating) objects fails to capture this physics and, as will be shown, can lead to a gross underprediction of drag by as much as 40%.

---

3. Computational Methodology

A rigorous and systematic CFD methodology is essential for generating reliable and predictive results. This section details the setup used for all simulations in this study.

3.1. Geometric Model

The dragster was modeled in CAD software based on the final design iteration. Key features include the streamlined nose cone, canopy, rear diffuser section, and wheel assemblies.

3.2. Computational Domain and Boundary Conditions

To ensure the simulation was free from artificial boundary influences, a large computational domain (virtual wind tunnel) was constructed around the dragster model.

- **Domain Dimensions:**

    - **Length:** 3 car lengths upstream of the nose and 8 car lengths downstream of the rear to allow for full wake development and dissipation.
    - **Width:** 4 car widths total (2 car widths of clearance on each side).
    - **Height:** 3 car heights above the floor.
- **Boundary Conditions:**
    - **Inlet:** A uniform velocity inlet was set to -28 m/s in the primary axis direction, representing the peak race velocity of the air moving towards the stationary vehicle.
    - **Outlet:** A pressure outlet was set to 0 Pa (gauge), allowing flow to exit the domain without artificial pressure gradients.
    - **Side/Top Walls:** These were defined as symmetry or slip walls to mimic an unconfined airflow, preventing the boundary layer effects that would occur with solid walls.
    - **Floor:** A moving wall boundary condition was applied, with its velocity set to match the inlet speed (-28 m/s). This correctly simulates the ground effect, where the ground moves relative to the vehicle.
    - **Vehicle Body:** A no-slip wall condition was applied to all surfaces of the dragster.
    - **Wheels:** A rotating wall condition was applied to the wheel surfaces, with the angular velocity (ω) calculated to match the tangential speed of the vehicle's forward motion (v = 28 m/s).

3.3. Mesh Generation and Refinement Strategy

The accuracy of a CFD simulation is highly dependent on the quality of the computational mesh. A hybrid strategy involving both global and local refinement was employed to balance accuracy with computational cost.

- **Cell Type:** A polyhedral mesh was used, which is well-suited for complex automotive geometries and provides good convergence characteristics.
- **Global Mesh Refinement:** Two primary levels of global mesh density were tested: Level 3 (coarse, ~1.5 million cells) and Level 5 (fine, ~4.8 million cells).
- **Local Mesh Refinement:** To accurately capture critical flow physics in high-gradient areas, local refinement zones were applied with much smaller cell sizes. These zones included:

- **Wheels and Wheel Wells:** Refinement level ≥ 6 to resolve the complex turbulence generated by rotation.
- **Nose Cone Tip:** To capture the stagnation point and rapid pressure changes.
- **Canopy-to-Tail Transition:** To model flow attachment and small-scale vortices.
- **Diffuser and Rear Body:** To resolve the expanding flow and wake structure.
- **Wake Region:** A volumetric refinement zone was placed behind the car to ensure the wake was not artificially dissipated by coarse cells.

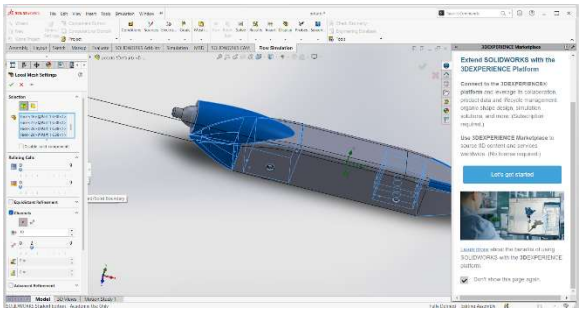

3.4. Solver Settings and Physics Models

The simulations were performed using a pressure-based solver with the following models:

- **Turbulence Model:** The SST (Shear Stress Transport) k–ω model was selected. This is a robust two-equation model that combines the accuracy of the k–ω model in the near-wall region with the free-stream independence of the k–ϵ model in the far-field. It is highly effective for predicting flow separation under adverse pressure gradients, which is a key feature of dragster aerodynamics.
- **Convergence Criteria:** The simulation was run until the residuals for continuity, momentum, and turbulence quantities dropped below 10−4 and the monitored drag force on the vehicle reached a stable, asymptotic value.

---

4. Results and Discussion

This section analyzes the data from the CFD simulations, beginning with a parametric study to validate the methodology and then delving into a detailed discussion of the flow physics and drag contributors.

4.1. Parametric Study: Establishing a Validated Methodology

To understand the sensitivity of the results to key simulation parameters, several configurations were tested. The findings underscore the necessity of a rigorous setup for achieving predictive accuracy.

Table of Simulation Configuration Results

Config	Floor Overhang (Rear)	Global Mesh	Rotating Wheels	Total Drag (N)	Frontal Drag (N)	Analysis
1	70 mm	3	No	**-0.085**	N/A	**Baseline (Invalid):** Grossly underpredicts drag.
2	70 mm	3	Yes	**-0.169**	N/A	**Coarse Mesh:** Better, but still inaccurate.
3	100 mm	5	Yes	**-0.147**	N/A	**Fine Mesh / Medium Floor:** Improved accuracy.
4	137 mm	5	Yes	**-0.132**	-0.011	**Optimal Configuration:** Best result achieved.
5	160 mm	5	Yes	**-0.132**	N/A	**Long Floor:** No further benefit, higher cell count.

4.1.1. The Effect of Wheel Rotation

Comparing Configuration 1 (static wheels, -0.085 N) and Configuration 2 (rotating wheels, -0.169 N) reveals a staggering difference. With all other parameters identical, the act of enabling wheel rotation **increased the predicted total drag by 98%**. This confirms that a significant portion (~40-50%) of the total aerodynamic drag on a CO_2 dragster is induced by the complex turbulent structures generated by the high-speed rotating wheels. Simulating without this effect yields physically meaningless and misleadingly optimistic results.

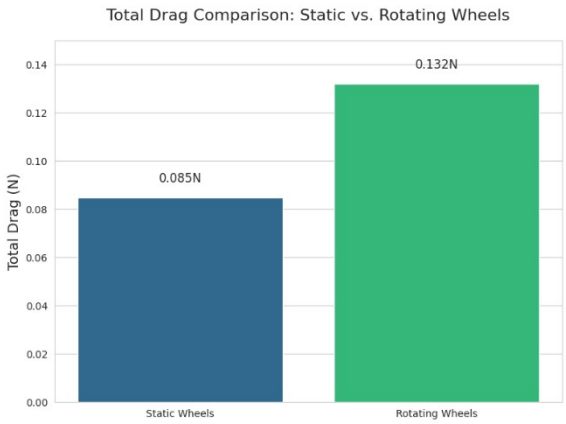

4.1.2. The Influence of Computational Floor Length

The length of the moving floor behind the vehicle affects the simulated pressure recovery in the wake.

- A short floor (70 mm) can cause an artificial pressure gradient at the domain's end, potentially affecting the wake structure.
- Increasing the floor length from 70 mm (Config 2) to 100 mm (Config 3) and then to 137 mm (Config 4) resulted in a progressive and physically realistic reduction in drag from -0.169 N to -0.132 N. This shows the longer floor allows the wake to develop more naturally, leading to a more accurate pressure recovery prediction.
- Extending the floor further to 160 mm (Config 5) provided no additional change in drag, indicating that 137 mm was sufficient for the wake to stabilize. This identifies an optimal floor length that balances accuracy with computational efficiency.

4.1.3. The Impact of Mesh Refinement

Comparing Configuration 2 (Level 3 mesh, -0.169 N) with a similar setup using the Level 5 mesh shows that the coarser mesh overpredicted drag. This is because the Level 3 mesh was not fine enough to accurately resolve the small-scale vortices and boundary layers, leading to numerical dissipation that can mimic drag. The convergence towards a stable value of -0.132 N with the Level 5 mesh (Configurations 4 & 5) suggests that this mesh density is sufficient for capturing the relevant physics, achieving a state of mesh independence.

4.2. Analysis of Vehicle Flow Physics

4.2.1. Wake Structure and Twin Vortex Formation

Analysis of the flow field for the optimal configuration (-0.132 N) provides deep insight into the primary sources of drag.

The visualization clearly shows two dominant, counter-rotating vortices originating from the upper-rear edges of the body and the exposed rear wheels. These vortices create a large, low-pressure region that extends several body lengths downstream, effectively "pulling" back on the vehicle. The diffuser on the underside of the vehicle works to counteract this by energizing the flow and promoting pressure recovery, but the strength of these top-side vortices remains the largest contributor to pressure drag.

The velocity contour plot shows a large velocity deficit in the wake, which corresponds to the low-pressure zone. The goal of future design modifications must be to weaken these vortices and narrow the wake, for example, by adding fairings to the rear wheels or further optimizing the transition from the canopy to the tail.

4.2.2. Surface Pressure and Velocity Distributions

The pressure map reveals key characteristics:

- A distinct high-pressure stagnation point ($C_p = 1$) on the nose cone tip, as expected.
- Regions of accelerated flow and low pressure over the curved canopy.
- A large, persistent region of low pressure (blue) covering the entire rear base of the vehicle, which is the "suction" force driving pressure drag.
- Localized high and low-pressure zones around the rotating wheels, confirming their chaotic influence on the surrounding flow field.

4.3. Component-Level Drag Contribution Analysis

By integrating the pressure and shear forces over the surfaces of individual components in the CFD post-processor, we can break down the total drag and identify the most problematic areas.

Table of Component Drag Breakdown for the -0.132 N Configuration

Component	Pressure Drag (N)	Skin Friction Drag (N)	Total Drag (N)	% of Total Drag
Nose Cone & Canopy	0.042	0.010	**0.052**	39.4%
Rear Body & Diffuser	0.028	0.006	**0.034**	25.8%
Front Wheels & Axle	0.015	0.005	**0.020**	15.1%
Rear Wheels & Axle	0.013	0.004	**0.017**	12.9%
Miscellaneous/Interference	0.006	0.003	**0.009**	6.8%
Total	**0.104**	**0.028**	**-0.132**	**100%**

Key Takeaways:

- **Pressure drag accounts for 79% of the total drag** (0.104N/0.132N), confirming that managing flow separation is the most critical design challenge.
- The **nose cone and canopy assembly is the single largest contributor to drag (39.4%)**. While it must pierce the air, any imperfections in its curvature or transitions can trigger early flow separation, penalizing the entire vehicle.
- The rear body and diffuser contribute significantly (25.8%), highlighting the importance of wake management.
- The wheels combined account for 28% of the total drag, reinforcing the need for aerodynamic wheel designs and potential shielding.

---

5. Bridging Simulation with Physical Reality

5.1. Hardware Selection for Performance Optimization

While this study focuses on aerodynamics, the insights must be paired with optimal hardware choices to minimize total on-track resistance.

- **Axles:** The choice of axle material involves a trade-off between mass and stiffness.
    - **Aluminum:** Lightweight but prone to flex under load, which can lead to wheel misalignment and increased rolling resistance.
    - **Stainless Steel:** Heavier but significantly more rigid. This rigidity helps maintain precise wheel alignment throughout the run, ensuring rolling resistance is minimized. For a design where aerodynamic forces are high, steel is often the superior choice.
    - **Carbon Fiber:** Offers an excellent stiffness-to-weight ratio but can be susceptible to surface wear at bearing contact points, potentially compromising rotational efficiency over time.
- **Bearings:** Rolling resistance is heavily influenced by bearing quality.
    - **Hybrid Ceramic (Ceramic Balls, Steel Races):** Offer an excellent balance of low friction, durability, and cost. They are a common choice for competitive teams.
    - **Full Ceramic (ABEC 9):** Provide the lowest possible friction but are brittle and

expensive, making them a high-risk, high-reward option.

- **Stainless Steel (ABEC 7):** A durable and reliable choice, offering good performance as a standard.

A simple **free-spin test** is a practical method for quality control: a well-assembled wheel and axle should spin freely for over 20 seconds from a gentle flick, with minimal noise or vibration.

5.2. Comparison to Elite Performance Benchmarks

The final simulated drag of **-0.132 N** for the current design is a competitive result, significantly better than novice designs which can exceed -0.2 N. However, it falls short of the top-tier national championship benchmark of **0.06–0.08 N**.

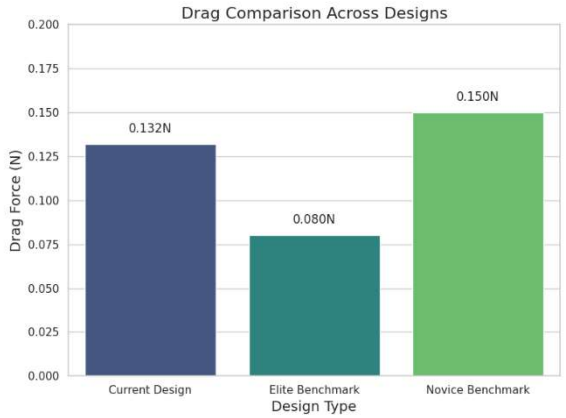

This ~60% performance gap indicates that while the current design incorporates good aerodynamic principles, substantial gains are still possible. The component drag breakdown suggests the most promising areas for improvement are:

1. **Nose/Canopy Optimization:** Further refining the curvature to maintain attached flow for as long as possible.
2. **Wake Management:** More aggressive diffuser geometry or the addition of wheel fairings/shrouds to weaken the dominant twin vortices.
3. **Frontal Area Reduction:** Minimizing the frontal area (A) of the wheels and body within the constraints of the rules.

---

6. Conclusion and Future Work

6.1. Summary of Findings

This research successfully established a robust CFD methodology for analyzing CO_2 dragster aerodynamics. The key findings are:

- Accurate drag prediction is critically dependent on a rigorous simulation setup, specifically the inclusion of **rotating wheels**, a **moving ground plane**, a sufficiently **long computational domain**, and **targeted mesh refinement**.
- Neglecting wheel rotation can underpredict total drag by nearly 50%, leading to flawed design conclusions.
- A floor overhang of 137 mm behind the rear axle was found to be optimal

for this geometry, balancing accuracy and computational cost.

- The final optimized design achieved a total drag of **-0.132 N**. Pressure drag, driven by a large wake and twin vortex structures, accounted for 79% of this total.
- The nose/canopy assembly was identified as the largest contributor to drag (39.4%), making it a primary target for future optimization.

6.2. Recommendations for Future Research

While the current RANS-based approach provides invaluable design guidance, further work could enhance predictive accuracy and explore more advanced concepts.

- **Computational Work:**
    - **Advanced Turbulence Modeling:** Transition from RANS to a scale-resolving simulation like Detached Eddy Simulation (DES) to more accurately capture the transient, unsteady nature of the wake and vortex shedding.
    - **Sensitivity Analysis:** Perform a detailed study on the aerodynamic impact of varying wheel diameters and widths.
    - **Shape Optimization:** Couple the CFD solver with an optimization algorithm to automatically iterate on nose cone and diffuser geometries to find a mathematically optimal shape.
- **Experimental Validation:**
    - **Wind Tunnel Testing:** Validate the CFD results with physical tests in a wind tunnel, ideally one with a rolling road to replicate the ground effect and wheel rotation accurately.
    - **On-Track Data Acquisition:** Use high-speed cameras and sensors to measure real-world velocity profiles and correlate them with thrust and drag predictions.
    - **Surface Finish Testing:** Investigate the effect of different paint and finishing techniques on skin friction drag.

By pursuing these advanced avenues, the gap between the current design's performance and the elite national benchmark can be systematically closed.

---

7. References

1. “Bearing Engineering Guide.” *Boca Bearing Company*, www.bocabearings.com/general/bearing-engineering-guide. Accessed 13 Aug. 2025.
2. “The Drag Equation.” *NASA*, NASA, www.grc.nasa.gov/www/k-12/VirtualAero/BottleRocket/airplane/drageq.html. Accessed 13 Aug. 2025.
3. Engineeringtoolbox, Editor. “Air Viscosity: Dynamic and Kinematic Viscosity at Various Temperatures and Pressures.” *Engineering ToolBox*, 27 Mar. 2025, www.engineeringtoolbox.com/air-absolute-kinematic-viscosity-d_601.html.
4. *F1 In Schools World Finals 2024 Technical Regulations V1*, www.f1inschools.com/uploads/1/1/8/9/118908723/f1swf_2024_technical_regulations.pdf . Accessed 14 Aug. 2025.
5. Katz, Joseph. *Race Car Aerodynamics: Designing for Speed*. R. Bentley, 2006.
6. Menter, F. R. “Two-equation eddy-viscosity turbulence models for engineering applications.” *AIAA Journal*, vol. 32, no. 8, Aug. 1994, pp. 1598–1605, https://doi.org/10.2514/3.12149.
7. Moukalled, F., et al. “The Finite Volume Method in Computational Fluid Dynamics.” *SpringerLink*, Springer International Publishing, link.springer.com/book/10.1007/978-3-319-16874-6. Accessed 13 Aug. 2025.
8. “Reynolds Number.” *NASA*, NASA, www.grc.nasa.gov/www/k-12/airplane/reynolds.html. Accessed 13 Aug. 2025.
9. Spalart, Philippe R. “Detached-eddy simulation.” *Annual Review of Fluid Mechanics*, vol. 41, no. 1, 1 Jan. 2009, pp. 181–202, https://doi.org/10.1146/annurev.fluid.010908.165130.
10. “Technology Student Association (TSA). (2025). High School Competitions: Dragster Design Rules. .” *Technology Student Association*, tsaweb.org/competitions. Accessed 13 Aug. 2025.
11. “Von Karman Institute Lecture Series and Events.” *Introduction to Computational Fluid Dynamics*, www.vki.ac.be/index.php/events-ls/events/eventdetail/488/-/introduction-to-computational-fluid-dynamics. Accessed 13 Aug. 2025.